Wholefield Optical Metrology:

Surface Profile Measurement

C.R. Coggrave

Phase Vision Ltd
http://www.phasevision.com/

1 Introduction ... 2
2 Computer vision techniques ... 5
3 Photogrammetry ... 7
4 Contouring speckle interferometry ... 9
5 Low coherence interferometry ... 11
6 Fourier transform speckle profilometry ... 13
7 Spectral interference microscope ... 15
8 Coaxial coimage plane projection and observation profilometry ... 16
9 Binary coding of projected structured light ... 17
10 Spatial frequency scanning of projected structured light ... 19
11 Multiplexed spatial frequency of projected structured light ... 22
12 Summary ... 23
13 Figures ... 25
14 References ... 30

1 Introduction

Conventional methods of measuring physical parameters such as surface strain, displacement, and profile utilise strain gauges, dial gauges and other mechanical or electrical sensing devices. Although these point-wise methods can potentially produce high-precision measurements their drawbacks include the requirement for contact with the surface under test and the localised measurement area. In general, large numbers of separate measurements are required to build up an overall picture of the physical parameter, however, when the required number of sensors exceeds 10^2-10^3 the cost typically becomes prohibitive. There has thus been much interest in developing *whole-field* (or full-field) non-contact metrology techniques that are able to provide measurements over large areas of the object surface at any one time to overcome the laborious procedure of point-wise measurement. Optical metrology methods such as speckle interferometry and optical profilometry provide an attractive solution for many applications and can provide whole-field information equivalent to more than 10^5 independent point-wise sensors. Sophisticated digital cameras with high spatial resolution (i.e. number of pixels), high temporal resolution (i.e. frame rate), and high accuracy (i.e. number of bits) have in many applications replaced photographic plates, thus enabling optical techniques to be adopted more easily.

Whole-field optical metrology is a broad subject area encompassing the measurement of physical properties of smooth or rough objects that can be opaque or transparent. The scope of this paper is limited, however, to engineering interest in surface profile measurement of *opaque* objects. Applications are introduced that provide a wide choice of sensitivities and dynamic range. Coherent optical methods are well suited for metrology applications requiring high precision but many techniques are only able to operate over a small dynamic range. In some applications, such as testing the flatness of diffuse surfaces, this does not pose a significant problem, however, there are other situations where an extended dynamic range is required. Whilst coherent interferometry are widely used for surface profile measurement, incoherent optical methods can also provide very practical solutions, and are particularly suitable for profiling applications where large surface height variations and discontinuities are encountered. These techniques enable measurement of deep surfaces where dynamic range is regarded as being as important as measurement sensitivity.

Techniques presented in this paper have been developed for the three dimensional description of deep surfaces and their position in space. Most surface profiling systems trade off measurement accuracy for dynamic range and in general are less sensitive than interferometry techniques used for measuring surface displacement. The methods described here, for example, have measurement sensitivities ranging from 10^{-6} m to 10^{-2} m. However, there is a recognised requirement in industry for optical techniques than provide both high dynamic range and high precision. Applications for these systems include automated manufacturing, quality control, robotic vision, and solid modelling[1].

Non-contact measurement of surface profile is usually dependent on techniques based on image cues, triangulation, various interferometric methods (including wavelength change, displacement of the test surface, and shifting the illumination beams) and projection of structured light patterns. These techniques can be divided into the broad categories of *passive* or *active* sensors. Passive profile sensors are typically less invasive than active methods and remotely measure the test surface profile under natural illumination by examining image cues such as shading or texture. By contrast, active methods typically require temporal control of the illumination, focus, or relative position of the test surface, and purposively adjust this parameter during the measurement process to increase the dynamic range whilst maintaining measurement accuracy.

Surface profilometry has been evolving as a subject for about thirty years and compiling an exhaustive list of all of the available methods is difficult to collate due to its vast, multidisciplinary, and continuous expansion. There is more to profilometry than can be covered in this paper, and therefore only the most widely used whole-field techniques that are suitable for automation are introduced. This paper does not discuss whole-field optical profilometry methods based on physical scanning of point-wise detectors, such as optical laser scanners for example, and the reader may refer to a recent paper Amann et al.[2] that provides a critical review of such techniques. In addition, Chen et al.[1] have recently published an overview of whole-field optical metrology methods for shape measurement.

The following discussion begins with an introduction to *computer vision* techniques for shape measurement. In practice these methods tend to have quasi real-time constraints and are suitable only for obtaining broad characterisation of surface properties. The remaining *range imaging* methods described in this paper have been developed to determine surface profile with accuracy several orders greater than that attainable by computer vision methodology, and furthermore, may also be suitable for quasi real-time applications. In general, the range imaging methods vary one or more of the system parameters over the measurement period to extend dynamic range whilst maintaining high accuracy.

Profiling of complex objects requires registration from different views, resulting in point clouds related to different co-ordinate systems. Precise transformation of these point clouds from each of the individual sensor co-ordinate systems into a common global co-ordinate system is therefore required to accurately characterise the complete surface. Several approaches are currently used to determine the relative orientation of the sensors including: (a) positioning using high-precision mechanical actuators and transducers (for example, the FaroArm manufactured by Faro Technologies Inc. enables multi-axis positioning), (b) statistically matching of point cloud data by optimal fitting[3], and (c) photogrammetric matching of point cloud data[4].

2 Computer vision techniques

Several techniques for determining surface profile fall into the domain of *computer vision* (also known as *scene analysis* or *image understanding*). In general, it is not possible to obtain depth information directly from two-dimensional intensity images, and it is therefore necessary to invert the many-to-one imaging transformation that maps points in the scene on to an image plane. In general, this recovery process requires knowledge of the objects in the scene and the projection geometry.

The *shape-from-texture*[5] method exploits variation in the size, shape, density, and aspect ratio of texture primitives to provide clues for the estimation of surface orientation and ultimately surface profile of scene objects. For successful measurement, the detector must be able to resolve the surface texture such that texture primitives can be distinguished. In practice, however, automated delineation of the primitives is extremely difficult for complex objects and the technique is thus only suitable for simple surfaces, or surfaces for which the texture is well characterised.

Exploitation of variations in image intensity due to changes in surface slope and a-priori knowledge of the *reflectance map* can be used to determine the surface position and orientation. The reflectance map specifies the intensity of surface patches at particular orientations for a given distribution of illumination and surface material. The basic technique, known as *shape from shading*, uses a single light source, however, unambiguous solutions are generally only obtained when the number of degrees of freedom can be reduced by assuming that the scene is composed of diffuse, smooth, continuous surface patches. *Photometric stereo* extends the technique by using several light sources. When a diffuse surface is illuminated by a point source, the lines of constant intensity in the image can be described by second-order polynomials. The set of surface orientations that can generate a given polynomial are restricted to those that lie along a curve in the reflectance map. A minimum of three independent point sources is therefore required such that the intersection of these curves unambiguously defines the surface orientation.

Another popular technique is *stereo vision* (also known as *binocular vision*), in which depth information is extracted from a pair of images obtained using two cameras displaced from each other by a known baseline distance. The simplest model uses two identical cameras arranged so that their image planes are coplanar. A feature in the scene is viewed by the two cameras at different positions in the image plane, separated by a *disparity* vector. Depth information can be recovered by identifying the disparities of corresponding image points (known as *homologous points*). Increasing the baseline distance enhances the accuracy of the depth calculation, however, it may also introduce other errors (e.g. distortions introduced by the perspective projection). There has been much research[6] applied to the detection and matching of features in the image pairs using methods such as edge matching, region correlation, and multiple primitives. This *correspondence problem* remains the main factor limiting adoption of the technique.

A further method known as *shape-from-focus* exploits the finite depth of field of optical systems to recover depth information[7]. The image is modelled as a convolution of focused images with a point spread function determined by the camera parameters and distance of the object from the camera. However, such reconstruction problems are mathematically ill posed, and height information can only be recovered in those regions where surface features are present.

3 Photogrammetry

Crossing over from the discipline of computer vision, *photogrammetry* techniques for determining three-dimensional information pursues higher levels of reliability and accuracy. Photogrammetry typically extends, but is not restricted to, the stereo vision method and developed almost exclusively for mapping large geographic areas in the domain of civil engineering and remote sensing. The advent of low cost digital cameras and software for automated image analysis has made the technique more attractive for application to close range measurement problems.

The starting point for building a close range photogrammetry model is the *central perspective projection* as shown in figure 1. The primary Cartesian co-ordinate system (XYZ) is located arbitrarily in object space and the secondary co-ordinate system (xyz) has its origin at O; its z-axis coincides with the principal axis POp and is directed away from the projection plane; its x- and y-axes are parallel to the projection plane. A point $A(X_A, Y_A, Z_A)$ in the three-dimensional object space is projected to point $a(x_a, y_a, -c)$ on the projection plane by a straight line AOa passing through the *perspective centre* O. The distance Op from the perspective centre to the projection plane is the *principal distance* denoted by c. The transformation mapping primary co-ordinates to secondary co-ordinates is given by the *collinearity equations*,

$$x_a = \frac{-c\left[r_{11}(X_O - X_A) + r_{12}(Y_O - Y_A) + r_{13}(Z_O - Z_A)\right]}{\left[r_{31}(X_O - X_A) + r_{32}(Y_O - Y_A) + r_{33}(Z_O - Z_A)\right]} \tag{1}$$

$$y_a = \frac{-c\left[r_{21}(X_O - X_A) + r_{22}(Y_O - Y_A) + r_{23}(Z_O - Z_A)\right]}{\left[r_{31}(X_O - X_A) + r_{32}(Y_O - Y_A) + r_{33}(Z_O - Z_A)\right]} \tag{2}$$

where r_{ij} are the elements of the rotation matrix R that maps the primary axes onto the secondary axes. The object space co-ordinates (X_A, Y_A, Z_A) of target A cannot be determined unambiguously from the photo co-ordinates (x_a, y_a) since the reverse transformation does not provide a unique solution. A measurement is analysed from a least two positions, yielding four measurement values; the redundant value can be used for both instant determination of object co-ordinates and model parameters. In general, three-dimensional reconstruction is based on the *bundle adjustment* principle. A geometric model of the camera positions and scene co-ordinates is developed analytically from the orientation of bundles of light rays and the optimal solution is found using a least squares minimisation approach. To determine the scale, only a single distance in the object space must be known. The technique enables *self-checking* of the data quality and *self-calibration* (i.e. simultaneous determination of co-ordinates and system parameters) to be performed, removing the need for expensive standards as used in conventional calibration procedures. Accuracies as high as 1 part in 1,000,000 have been reported[8], however, calculations are often time-consuming. In general markers must be attached to the test surface as homologous points to aid in solving the correspondence problem unambiguously. Recent work by Reich et al.[4] has combined photogrammetry and fringe projection to solve the correspondence problem by projecting coded fringes with different orientations onto the test surface.

An excellent introduction to close range photogrammetry is provided by Atkinson[6] and there are several books which cover the general technique[9,10].

4 Contouring speckle interferometry

Although speckle interferometry is most often encountered in the domain of surface displacement analysis, several methods based on speckle interferometry have been developed for measuring surface profile. These methods generally vary one of a number of parameters controlling the fringe formation against time, including: (a) illumination direction (described below); (b) temporal coherence (for example, see section 5); and (c) optical wavelength (for examples, see sections 6 and 7).

The electronic speckle contouring (ESC) method is based on conventional in-plane and out-of-plane displacement sensitive arrangements where small changes in the illumination direction are introduced. Rodriguez-Vera provides useful state-of-the-art review of ESC methods in reference[11]. Zou et al.[12] and Rodriguez-Vera et al.[13] describe a dual-beam arrangement for measuring surface profile in which the surface remains unchanged and the illumination beams are shifted to vary the sensitivity vector during the experiment. Joenathan et al.[14] describe an analogous arrangement in which the object is tilted to induce a relative shift in the illumination directions. The latter method uses an arrangement that is similar to the in-plane displacement set-up (figure 2), with the addition of a rotation stage on which the test surface is mounted. The illumination beams are arranged symmetrically about the normal ($\theta = \theta_1 = \theta_2$) such that the interferometer is only sensitive to the in-plane displacement component u. Correlation fringes are formed from the speckle interferograms recorded before and after a small rotation of the surface. The in-plane displacement component u produced by a rotation ω is dependent on the surface height h, and therefore the resultant fringes represent surface height contours.

Consider the arrangement shown in figure 3(a). The surface is rotated about an axis parallel to the y-direction and passing through point O. The so-called tilt plane TP is defined as the plane passing through the axis of rotation in which the in-plane displacement is zero (i.e. perpendicular to the line of sight). The point $P(x, y, z)$ on the surface, located at height h in front of the tilt plane, is displaced by the rotation to $P'(x + \Delta x, y, z + \Delta z)$. Geometry analysis (see figure 3(b)) reveals that the in-plane displacement component $u(P)$ is given by

$$u(P) = 2r\sin(\omega/2)\cos(\alpha - \omega/2) \tag{3}$$

where r is the radial distance between O and P. Substituting $r = \dfrac{h}{\cos\alpha}$ gives

$$u(P) = \frac{2h\sin(\omega/2)\cos(\alpha - \omega/2)}{\cos\alpha} \tag{4}$$

For small angles of rotation ω, the in-plane displacement is approximately proportional to the surface height and angle of tilt

$$u(P) \approx h\sin\omega \tag{5}$$

The change in speckle phase $\Delta\phi(P)$ contributed by point P, due to rotation of the test surface is then given by

$$\Delta\phi(P) = \frac{4\pi}{\lambda} h\sin\omega\sin\theta \tag{6}$$

Coherence fringes thus represent surface height contours separated by $h = \lambda/(2\sin\omega\sin\theta)$, where the dependence on θ enables the height sensitivity to be controlled simply by changing the illumination directions. Fringe modulation is maximised by reducing speckle decorrelation and therefore small tilt angles should be used. Height contour sensitivity can be enhanced by a factor of N simply by modulo-2π addition of the phase changes due to N small tilt increments.

The close relationship between speckle interferometry and holography means that the same principles can be extended to the holography domain, in which the chosen parameter is altered between constructions of the two wavefronts. Holographic optical arrangements have been developed for contouring by shifting the illumination direction[15-19], by altering the refractive index of the surrounding medium[20] (also called the immersion method), and by wavelength differences[21-28].

5 Low coherence interferometry

Temporal coherence describes the correlation of a wave with itself as a function of distance along the direction of propagation. Although the degree of coherence cannot be measured directly, it can be determined from the fringe contrast, which is measurable. For waves of equal intensity, the degree of coherence is numerically equal to the contrast V

$$V = \frac{I_{\max} - I_{\min}}{I_{\max} + I_{\min}} \qquad (7)$$

where $I_{\max}$ and $I_{\min}$ are the maximum and minimum intensity, respectively. In other cases additional terms are introduced[29]. The coherence time τ_c is defined as the time shift at which the contrast falls to $1/e$. In interferometers, for example, each arm has a different optical path length and therefore introduces a time shift between the two light waves and it is useful to define the coherence length $l_c = c\tau_c$.

Dresel et al.[30] described a technique known as *coherence radar* (also called *low-coherence interferometry*) that exploits the coherence length of a given light source to measure surface profile. The technique is based on the generation of white-light fringes by nulling the optical path differences caused by the surface height distribution. The arrangement (figure 4) is based on a Michelson interferometer with one of the mirrors replaced by the test surface that is mounted on a mechanical translation stage. Mirror M is mounted on a piezoelectric transducer (PZT) to enable phase shifting. A light source with a short coherence length is required for accurate measurement, typically a laser diode, a LED, or incandescent lamp. The short coherence length restricts interference to those speckles that correspond to the surface elements close to the plane R where the optical path lengths of the interferometer arms balance. The intensities of the interfering waves must be equal for maximum contrast and therefore a neutral density filter is introduced into the reference arm to compensate for scattering at the test surface. The imaging lens is adjusted so that plane R is focused onto the detector.

During the measurement process the test surface is slowly translated along the z-axis. For a given offset, $h(t)$, along the z-axis, the reference arm is phase stepped using the

PZT and the contrast $V(x, y, t)$ calculated independently for each pixel from the measured intensities. The surface height at each pixel is then determined by detecting the offset $h_{\max}(x, y)$ required for maximum contrast at each pixel. It should be noted that this method does not measure the phase of the interference, but merely identifies that coherent interference is occurring.

Since the illumination and observation directions are parallel the technique does not suffer from shading problems. In addition, the measurement accuracy is independent of aperture setting (unlike shape-from-focus methods for example) and measurement distance so the technique is well suited to surfaces with deep narrow holes. For practical broadband light sources the illumination aperture should be smaller than the observation aperture to maintain spatial coherence. Accurate mechanical movement of the object and reference mirror is required, and interferometer alignment may become a critical issue for large translations. The measurement process can be time consuming: a total translation of 5 cm, for example, by steps smaller than the coherence length (e.g. 2 μm) requires a repetition of more than 25,000 step movements of the test surface, with phase shift measurements made at each step.

6 Fourier transform speckle profilometry

Fourier transform speckle profilometry (FTSP) suggested by Takeda et al.[31] is based on the combination of wavelength-shift speckle interferometry[32] and the Fourier-transform technique (FTT) for temporal fringe pattern analysis. The technique overcomes some of the shortcomings of coherence radar since it does not depend on the accurate mechanical translation of the surface and reference mirror, thus reducing hardware costs and measurement time. The optical arrangement (figure 5) is similar to that used for coherence-radar but uses a coherent frequency-tuneable laser diode as the light source. The test surface is placed in one of the interferometer arms such that the half optical path difference $l(x, y)$ depends on the surface height. The basic technique scans the laser diode injection current so that the wave number $k(t) = \alpha t + \kappa(t)$ varies quasi-linearly with time, where α is a constant and $\kappa(t)$ represents an initial wave number $k(0)$ plus an unavoidable deviation from perfect linearity. Wavelength scanning causes the intensity of each speckle to vary sinusoidally giving the illusion that the speckle pattern is "boiling"; the rate of intensity variation is proportional to the optical path difference. The time-varying specklegram is of the form

$$g(x, y, t) = a(x, y, t) + b(x, y, t)\cos\left[2k(t)l(x, y)\right] \tag{8}$$

where $a(x, y, t)$ and $b(x, y, t)$ are, respectively, the background intensity and the fringe amplitude, that unavoidably change with the injection current. Substituting for $k(t)$ gives equation 9 that describes an amplitude- and phase-modulated sinusoid with a temporal carrier frequency $f_0(x, y)$,

$$g(x, y, t) = a(x, y, t) + b(x, y, t)\cos\left[2\pi f_0(x, y)t + \phi(x, y, t)\right] \tag{9}$$

where

$$f_0(x, y) = \alpha l(x, y) / \pi \tag{10}$$

$$\phi(x, y, t) = 2\kappa(t) l(x, y) \tag{11}$$

The FTT provides a robust method for extracting the height information encoded in the temporal carrier frequency since it is immune to non-linearity of the injection current vs. wavelength characteristic and variations due to temperature. If we let

$c(x, y, t) = \frac{1}{2} b(x, y, t) \exp i[\phi(x, y, t)]$ then the Fourier transform of $g(x, y, t)$ with respect to the time variable t is given by

$$G(x, y, f) = A(x, y, f) + C[x, y, f - f_0(x, y)] + C^*[x, y, -\{f + f_0(x, y)\}] \qquad (12)$$

where * denotes the complex conjugate, the uppercase letters denote the Fourier spectra of the signals denoted by the corresponding lower case letters. Since the separation of these spectra is proportional to $l(x, y)$ it is necessary to arrange the interferometer with a large optical path difference between the arms to enable the spectra to be separated. One consequence of this increased path difference, however, is that the temporal sampling rate must also be increased to avoid aliasing problems. One of the sidebands is selected by filtering and the inverse Fourier transform computed to obtain the analytical signal $c(x, y, t)$. The complex logarithm is calculated to separate the amplitude- and phase-modulation terms. Finally, one-dimensional phase unwrapping along the time axis is required to recover $\phi(x, y, t)$, and thus obtain the height information.

As with the coherence radar technique, Fourier transform speckle profilometry is a line of sight measurement method and therefore does not suffer problems due to shading. However, some of the light scattered back from the surface of the object will not enter the interferometer and therefore some pixels may not contain valid profile information and must be masked from the result.

7 Spectral interference microscope

Commercial tuneable laser diodes tend to have many mode hops along the frequency axis that limit the continuous frequency scanning range available to FTSP systems and so restrict the achievable vertical measurement resolution to approximately 10^{-4} m. Attempts have been made to improve the resolution by use of more sophisticated lasers, such as an external cavity laser diode[33,34] and a dye laser[35,36] that have a wider tuneable range. However, these lasers are often expensive, and in the case of the dye laser relatively cumbersome due to the use of carcinogenic chemicals and water cooling.

The spectral interference microscope developed by Kinoshita et al.[37] provides an alternative solution by exploiting a frequency tuneable liquid crystal Fabry-Perot etalon device that acts as a very narrow band-pass filter. The device has been developed primarily for wavelength multiplexing communication applications and consists of a crystal with a partially mirrored surface on each end and transparent electrodes. An applied voltage in the range 3-5 volts changes the orientation of the molecules within the crystal and so controls the refractive index. As a direct result, the applied voltage can be used to conveniently control the pass-band of the Fabry-Perot filter.

Liquid crystal Fabry-Perot interferometers (LC-FPI) can be used together with inexpensive broadband light sources (e.g. LEDs and super luminescent diodes) to select the wavelength of interest. Reference [37] describes a LC-FPI used as an optical frequency scan device and designed with a nominal pass-band width of 1.1 nm at the central wavelength of 665 nm that can be varied over a nominal maximum range of 23 nm. The system is able to perform measurement on discontinuous microscopic surfaces without the use of mechanically moving components. In addition, the LC-FPI is physically very small and only requires low voltages to control the pass-band.

8 Coaxial coimage plane projection and observation profilometry

Interferometry contouring methods enable surface profiles to be measured without the baseline required for triangulation systems and therefore do not suffer from shading problems. However, these coherent processing systems are susceptible to vibration noise and air currents, which makes them unsuitable for adverse industrial environments. The coaxial coimage plane projection and observation technique proposed by Takeda et al.[38] combines the robustness of white light projection with the immunity to shading problems. The arrangement shown in figure 6 consists of a projection system that projects a grating pattern onto the conjugate image plane R, and an observation system that images plane R via a beam splitter onto the detector. Plane R is therefore a coimage plane for both the projection and observation systems that are arranged coaxially to eliminate shading problems. As the test surface is moved through the conjugate plane R using a high precision translation stage the contrast of the detected fringe pattern varies, with the peak contrast occurring where the scattering surface crosses the plane R. The surface height is therefore determined by detecting the translation required for maximum contrast at each pixel.

This arrangement can be regarded as a depth-from-focus technique, however, it differs from conventional depth-from-focus methods that rely on the spatial information of the surface itself rather than projected spatial information, and exclusively defocus the observation optics. The use of projected grating patterns enables profiling of non-textured surfaces and, furthermore, the reduced depth of focus of the combined imaging system provides an improvement in the measured height resolution. One of the main advantages of this arrangement over projection systems that require a finite baseline is that problems due to shading are significantly reduced. Note, however, that this is arrangement cannot be regarded as a “true” line-of-sight technique since a finite range of angles along the coaxial projection and observation direction are required to provide a finite depth-of-field.

9 Binary coding of projected structured light

Interferometric techniques discussed in the previous sections are able to achieve very accurate measurements over small depth ranges but are unsuitable for medium- and long-range applications. *Active structured light* methods based on triangulation (also categorised as active triangulation methods) are widely used in this interval and use a projection unit to illuminate the scene with a known light pattern coming from a known angle relative to the viewing angle.

In locating a point $P(X,Y,Z)$ on the test surface, the camera pixel co-ordinates (x,y) determine two of the three degrees of freedom and the projector is used to label the third. To determine surface height it is sufficient to label planes in space and this is achieved by projecting structured light patterns onto the test surface. The projection of lines can be regarded as light sectioning planes that label the measurement volume as illustrated in figure 7. In general, the sections are labelled by the intensity of the illumination, however, other methods have been reported (see reference[39], for example). The number of sections that can be labelled by a given projection in a single image is therefore limited by number of different intensities of light that can be generated. Projection of a temporal sequence of intensities for each lighting section enables the dynamic range to be extended. The sequence of intensities can be regarded as a code that uniquely identifies a given section. In addition to the measured intensity values, parameters describing the geometrical conditions of the sensor enter into the co-ordinate calculation. These parameters are normally determined in a calibration procedure before actual three-dimensional measurement begins.

The choice of coding scheme influences the speed and resolution of the measurement and several approaches have been reported (see references [40,41] for example); the most common schemes employ *n*-bit binary codes (i.e. the projected stripe is either "on" or "off") and allow the unique description of 2^n different light sections. An optimum coding scheme should: (a) be self normalising to simplify demodulation; (b) identify each light section uniquely; (c) only change one of the code digits between adjacent code-words (i.e. Hamming-distance equal to 1) to avoid decoding errors; and (d) utilise as many of the available code-words as possible to maximise efficiency. Several alternatives schemes, including the popular Gray-code and Lemming-code, are evaluated by Gartner et al.[42].

Binary coding of projected structured light provides a convenient technique for automation and several systems have been developed using liquid crystal spatial light modulators to generate the projection sequence. Increasing the number of codewords enables either the dynamic range or the resolution of measurement to be extended, however, this also increases the number of patterns that must be projected. The image analysis process can be regarded as a simple fringe counting method and as such the resolution is limited to integer fringe orders. Sansoni et al.[43] reported a technique to address this problem using the spatial phase shifting method to measure fractional parts of a code word; the technique has been adopted by most commercial profilometry systems based on binary coding available today. In general binary coding schemes are only practical for incoherent fringe projection systems and require high stability of the optical set-up to maintain pixel registration during the measurement period. As with all triangulation techniques a finite baseline is required between the projector and the camera that may introduce shading problems in the acquired images. Furthermore, measurement of dynamic events requires expensive high-speed projection and imaging hardware.

10 Spatial frequency scanning of projected structured light

Projected structured light techniques using projected gratings with sinusoidal intensity distribution are based on the extraction of the continuous phase parameter to identify the projection plane (see figure 8). The achievable measurement resolution is therefore not restricted by a finite number of codewords as seen with the binary coding approach. When a grating pattern is projected at an angle to the observation direction on to a surface the fringes are perturbed according to the topography and can be regarded as a phase-modulated pattern with a constant spatial carrier. Demodulation of the deformed grating by means of a matched reference grating results in the well-known moiré fringe pattern[44] and enables very accurate measurement of surface profile[45]. Several automated methods for quantitative analysis of the moiré fringes have been described[46,47], however, the sign of the depth information cannot be determined unambiguously. Xie et al.[48,49] describe a simple extension to the shadow moiré technique that enables absolute height information to be determined by rotation of the grating. Several alternative approaches to moiré contouring based on analysis the deformed grating itself rather than the moiré pattern have been developed[50] and therefore determine surface height unambiguously[31,51,52].

Considering the general non-telecentric divergent projection geometry shown in figure 9, point P is the centre of the exit pupil of the projector lens and point I is the centre of the entrance pupil of the imaging lens separated by distance d_0. The crossed optical axes of the projection and imaging lenses lie in the same plane and intersect making an angle θ at point O on a fictitious plane R. Plane R, normal to the optical axis of the imaging lens, serves as a reference from which surface height $h(x, y)$ is measured. We define the co-ordinate system (x, y) lying in the fictitious plane R with the origin at O. If the uniform grating image falling on to the plane Q perpendicular to the projection axis has a constant spatial frequency $f = \lambda^{-1}$, then the fringe period of the grating image $g_0(x, y)$ viewed on plane R will increase as point C on the *x*-axis departs from the origin. Grating intensity $g_0(x, y)$ is described by a spatial carrier frequency f_0 phase-modulated by $\varphi_0(x)$,

$$g_0(x) = a_0(x, y) + b_0(x, y)\cos[2\pi f_0 x + \varphi_0(x)] \tag{13}$$

where $f_0 = \lambda_0^{-1} = \lambda^{-1}\cos\theta$ and $\varphi_0(x) = 2\pi f_0 \overline{BC}$ equals the phase difference along length $\overline{BC}$. To evaluate $\overline{BC}$ we note that $\overline{BC} = \overline{OC} - \overline{OB}$ and let $\overline{OC} = x$. From the geometry we have $\overline{OB} = l_0 \tan\alpha \cos^{-2}\theta$ where $\tan\alpha = (x\cos^2\theta)(l_0 + x\sin\theta\cos\theta)^{-1}$. Substituting $\overline{OB}$ and $\overline{OC}$ gives $\overline{BC} = (x^2\sin\theta\cos\theta)(l_0 + x\sin\theta\cos\theta)^{-1}$ and hence,

$$\varphi_0(x) = \frac{2\pi f_0 x^2 \sin\theta\cos\theta}{l_0 + x\sin\theta\cos\theta} \tag{14}$$

When the grating is projected on to a general surface with height $h(x, y)$ the principal ray PCH strikes the surface at point H, and point H will be seen at point D on plane R when observed through the imaging lens. The deformed grating $g(x) = a(x, y) + b(x, y)\cos[2\pi f_0 x + \varphi(x)]$ encodes the height information in the phase-modulation term $\varphi(x) = 2\pi f_0 x\overline{BD}$. From the similarity of triangles ΔHCD and ΔHPI we obtain

$$h(x, y) = \frac{l_0 \overline{CD}}{d_0 - \overline{CD}} \tag{15}$$

Noting that $\overline{CD} = \overline{BD} - \overline{BC}$ we have $\overline{CD} = (2\pi f_0)^{-1}\Delta\varphi(x)$, and substituting into equation 15 gives,

$$h(x, y) = \frac{l_0 \Delta\varphi(x)}{2\pi f_0 d_0 - \Delta\varphi(x)} \tag{16}$$

where $\Delta\varphi(x) = \varphi(x) - \varphi_0(x)$ is the phase difference observed between the surface grating $g(x, y)$ and the reference grating $g_0(x, y)$.

Discontinuous surfaces may cause 2π ambiguity in the recovered phase unless the projected phase range across the surface is limited to a single fringe period, which severely limits the measurement accuracy. Practical systems overcome this problem by combining: (a) a phase shifting approach to determine the phase modulo 2π; and (b) a hierarchical approach to determine the missing integral multiple of 2π that must be added to obtain the absolute phase (equivalent to the determination of the correct fringe order at each pixel). The general principle consists of the generation of a synthetic spatial wavelength λ along the *x*-axis by tuning one of the flexible system parameters, for example: Saldner et al.[53] describe tuning the angle of one of the mirrors in a Michelson interferometer; Valera et al.[54] describe tuning the separation of two coherent fibre optic sources; Zhang et al.[55] describe tuning the orientation of a fixed grating in its own plane illuminated by incoherent light. The synthetic wavelength is scanned during the measurement procedure, increasing in a step-wise manner from a single fringe across the field of view, to obtain several phase maps at different sensitivities and thus enables improved accuracy whilst maintaining the dynamic range. Storage and subsequent interpretation of the large number of images produced by the technique can, however, require expensive hardware and significant computational effort.

Incoherent or coherent (interference) sinusoidal fringes can be used. Incoherent fringes are usually more convenient for projection on large objects but are strongly limited by depth of field of the projection optics. High-brightness, high-contrast sequences of computer generated fringe patterns can be projected at high speed using low-cost liquid crystal (LC) and digital mirror device (DMD) spatial light modulators, enabling optimisation of the fringes based on feedback of the acquired image sequence with only a small time penalty[56]. Coherent fringes introduce additional speckle noise but do not suffer from finite depth of focus and hence can be projected into an entire measurement volume. As with other coherent systems, however, coherent fringe projection is susceptible to noise vibration and air currents.

11 Multiplexed spatial frequency of projected structured light

Although discontinuous surfaces can be measured by binary coding and spatial frequency scanning of structured light patterns the time required to project and record multiple frames restricts their application to surfaces that are static or in relative slow motion. Takeda et al.[57] describe a technique based on projected structured light that requires only a single fringe pattern and permits phase unwrapping for discontinuous surfaces from a single acquired image. Rather than temporal scanning of the grating spatial frequency as described in section 10, multiple phase maps with various phase sensitivities are spatial-frequency multiplexed into a single fringe pattern to unambiguously determine the surface height. The acquired image is filtered in the two dimensional Fourier domain to demultiplex the spatial carrier frequencies, each of which has been phase modulated by the surface height with varying sensitivity. The phase is decoded using the Fourier transform technique but will be wrapped into the range $[-\pi, \pi]$. The unambiguous phase must then be determined from the simultaneous wrapped phase equations using a modified phase unwrapping method.

By virtue of its single-shot recording the technique is suitable for the instantaneous measurement of dynamic motion that would not be possible using sequential projection and recording of multiple structured light patterns. However, multiplexing of spatial frequencies in the projected light pattern reduces fringe contrast and introduces difficulties during phase extraction. In particular, filtering of the acquired image in the Fourier domain band-limits the broadband signal obtained for discontinuous surfaces, and therefore reduces the attainable signal to noise ratio compared to sequential projection and recording schemes.

12 Summary

This paper has presented a brief description of the most popular whole-field optical techniques for measuring surface profile. However, these represent only a small fraction of the wide range of optical arrangements that are described in the literature.

Techniques for surface profile measurement have been described offering various trade-offs between dynamic range and sensitivity. Close range photogrammetry enables measurement of large surface areas with the ability to self-calibrate and self-check; however, is unsuitable for real-time implementation due to the computational effort required. Contouring techniques based on interference provide very high accuracy over short measurement ranges. Contour speckle interferometry remains popular since the simple optical arrangement can also be used for surface displacement measurements. Low coherence interferometry utilises the short coherence length of white light illumination to determine the optical path length difference between interferometer arms and therefore does not suffer from shading problems making it suitable for surfaces with deep holes. However, contouring speckle interferometry and low-coherence interferometry both require expensive mechanical devices to accurately position the test surface relative to the optical arrangement which restrict the speed of data acquisition. Fourier transform speckle profilometry overcomes these limitations by use of a frequency tuneable laser diode that enables fast scanning of the optical wavelength, however, the height sensitivity is limited by the quasi-linear scanning range between laser mod-hops. A Fabry-Perot etalon is used to filter a broadband light source in the spectral interference microscope and therefore provides a wider scanning range that allows improved height sensitivity. Coherent measurement techniques are susceptible to air currents and noise vibration, thus making them difficult to deploy in industrial environments. The co-axial co-image plane projection and observation technique utilises incoherent grating projection to provide a more robust method for profile measurement that is free from shading problems, however, an accurate mechanical translation device is required to position the surface. Profile measurement in the medium- to long-range is dominated by active triangulation systems. Binary coding of sequences of projected structured light enables low-cost, high-speed characterisation of discontinuous surface profile, however, the accuracy is restricted by a finite number of codewords. Spatial frequency scanning of projected gratings overcomes this problem using the continuous phase parameter to identify projection planes. Spatial-frequency multiplexing of the projected gratings enables profile measurement of dynamic surfaces at the cost of reduced signal to noise.

Ultimately, the optical technique chosen to measure the physical property under test will depend on the required sensitivity and dynamic range.

13 Figures

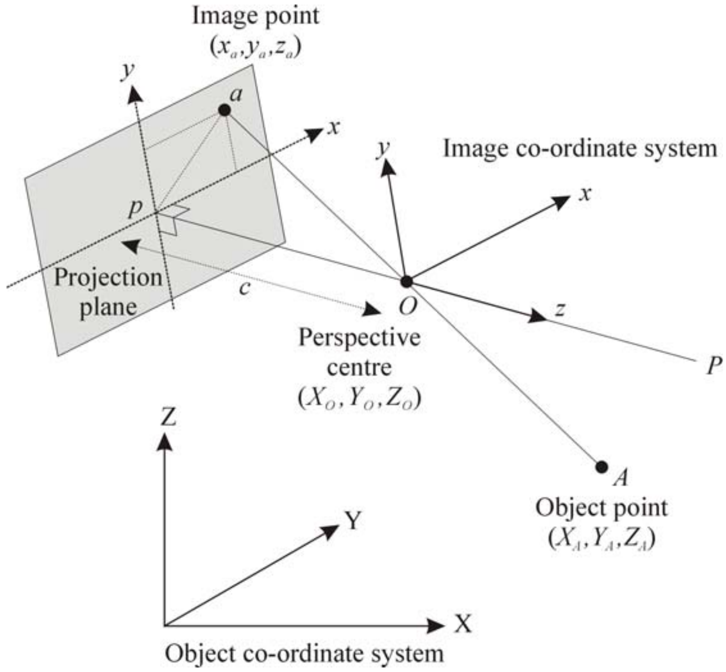

Figure 1: Central perspective projection

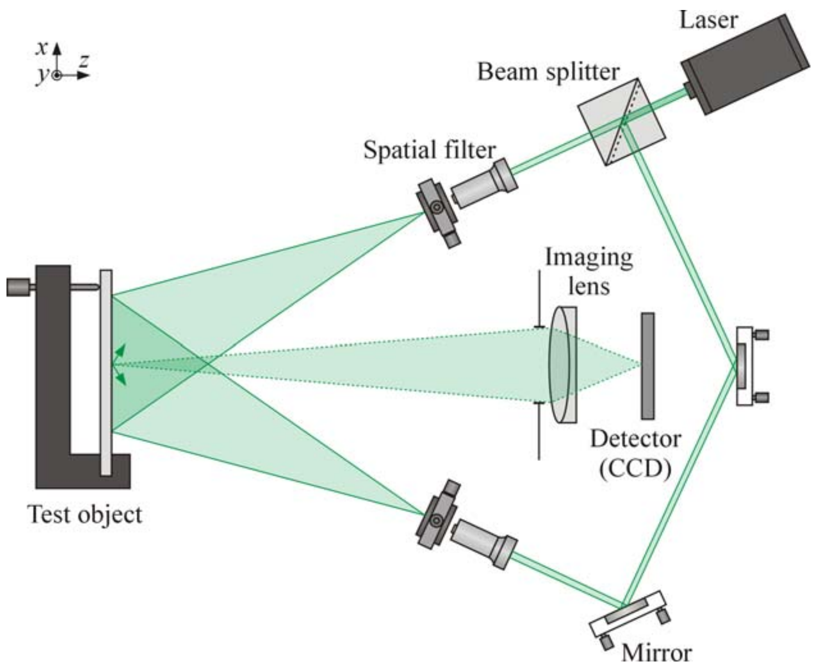

Figure 2: Optical arrangement for in-plane speckle interferometry

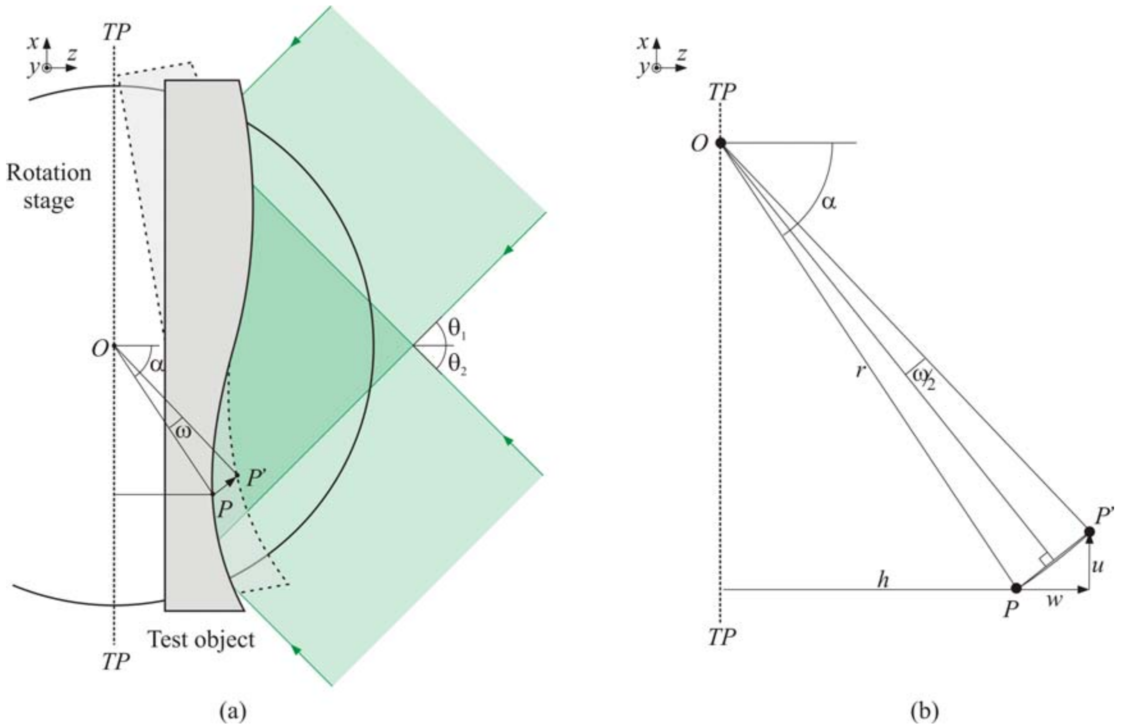

Figure 3: Optical arrangement for speckle contouring: geometrical analysis

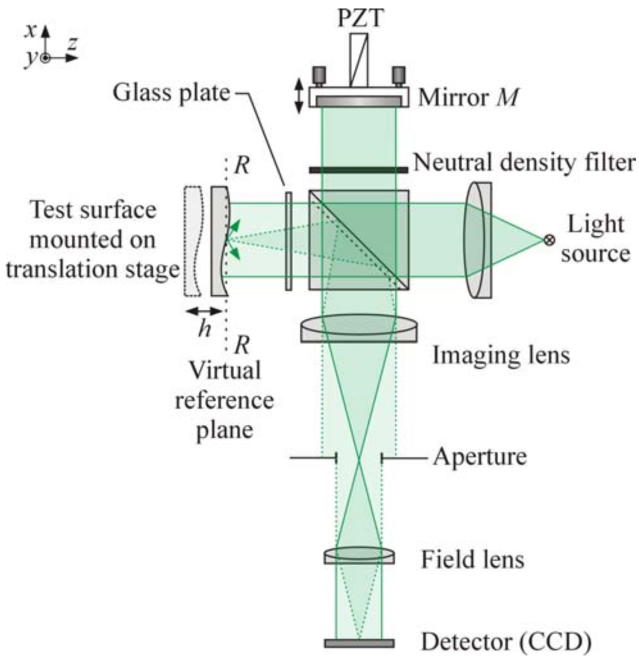

Figure 4: Optical arrangement for low-coherence interferometry

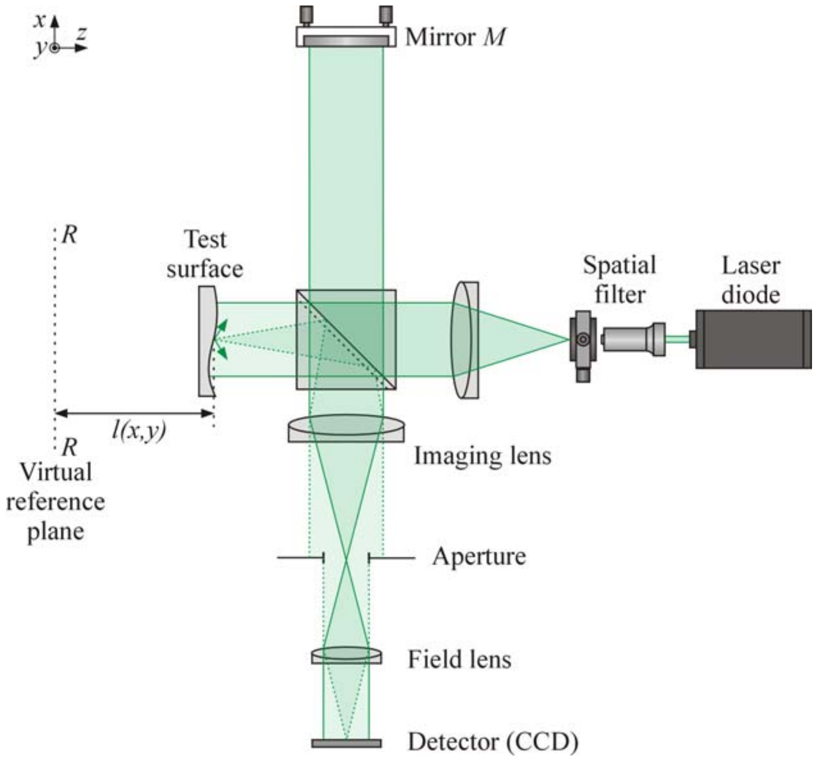

Figure 5: Optical arrangement for Fourier transform speckle profilometry

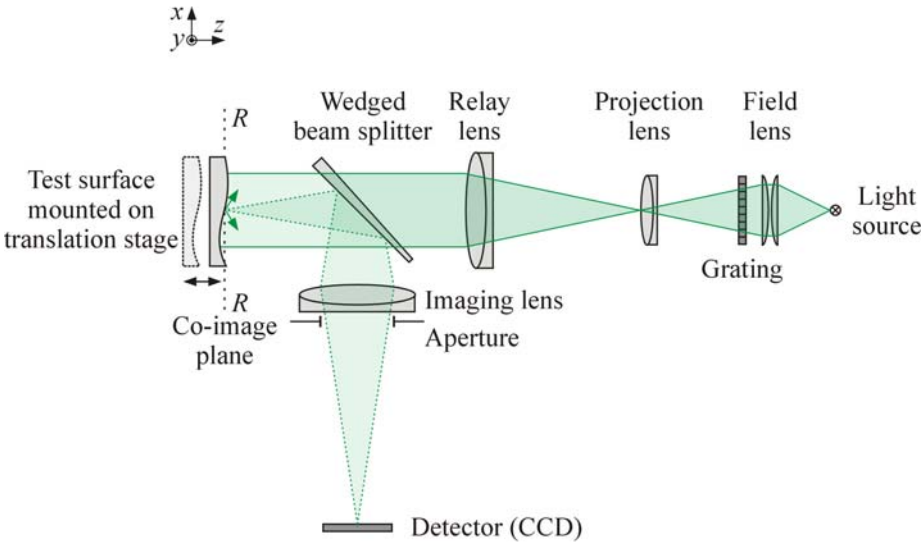

Figure 6: Optical arrangement for co-axial co-image plane projection and observation profilometry

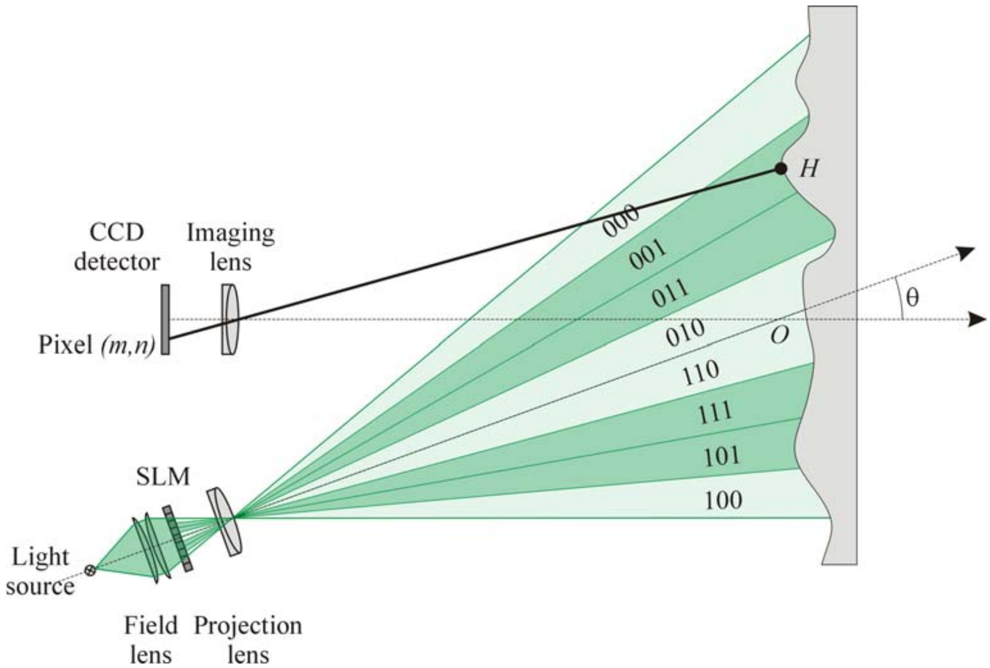

Figure 7: Optical arrangement for binary coding of projected structured light from a spatial light modulator (SLM) with crossed projection and imaging axes. Diagram shows one of a sequence of structured light patterns used in a 3-bit Gray code scheme to label the projection planes.

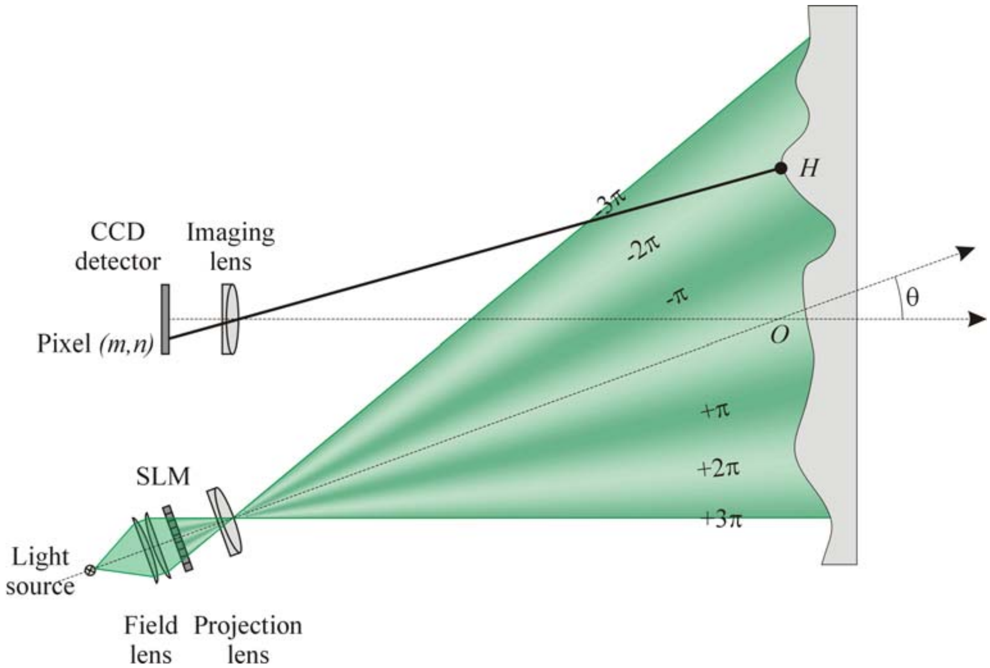

Figure 8: Optical arrangement for projected synthetic grating from a spatial light modulator (SLM) with crossed projection and imaging axes. Diagram shows one of a sequence of structured light patterns with zero phase on the projection axis and a uniform phase distribution from -3π to $+3\pi$ across the projection field.

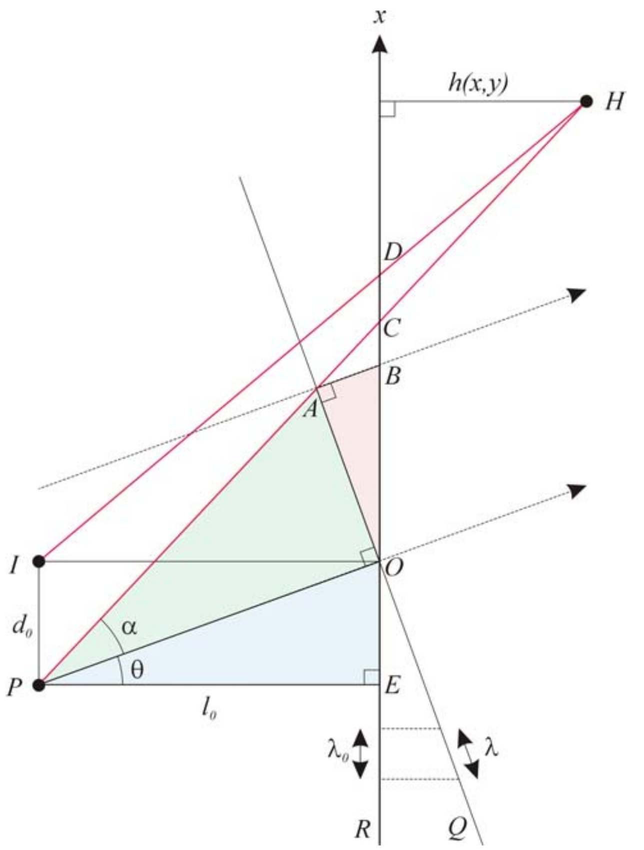

Figure 9: Optical geometry for projected structured light methods with crossed optical axes.

14 References

1. Chen F., Brown G.M., Mumin S. '*Overview of three-dimensional shape measurement using optical methods*', Optical Engineering **39**(1) 10-22 (2000).

2. Amann M.-C., Bosch T., Lescure M., Myllylä R., Rioux M. '*Laser ranging: a critical review of usual techniques for distance measurement*', Optical Engineering **40**(1) 10-19 (2001).

3. Li N., Cheng P., Sutton M.A., McNeill S.R., Chao Y.J. '*Accurate integration of surface profile data with quantitative error analysis*', Experimental Mechanics **41**(1) 77-83 (2001).

4. Reich C., Ritter R., Thesing J. '*3-D shape measurement of complex objects by combining photogrammetry and fringe projection*', Optical Engineering **39**(1) 224-231 (2000).

5. Witkin A.P. '*Recovering surface shape and orientation from texture*', Artificial Intelligence **17**(1) 17-45 (1981).

6. *Close Range Photogrammetry and Machine Vision*, Atkinson K.B. [Ed], Whittles Publishing, Latheronwheel, 1996.

7. Subhasis Chaudhuri, Rajagopalan A.N. *Depth From Defocus: A Real Aperture Imaging Approach*, Springer-Verlag, New York, 1998.

8. Fraser C.S. '*Photogrammetric measurement to one part in a million*', Photogrammetric Engineering & Remote Sensing **58**(3) 305-310 (1992).

9. *Manual of Photogrammetry*, Slama C.C., Theurer C., Henriksen S.W. [Eds], American Society of Photogrammetry, 4th ed, 1980.

10. Moffitt F.H., Mikhail E.M. *Photogrammetry*, Harper & Row, Cambridge, 3rd ed, 1980.

11. Rodriguez-Vera R. '*Optical gauging of diffuse surfaces by electronic speckle contouring*', Optics & Lasers in Engineering **26**(2) 101-114 (1997).

12. Zou Y., Diao H., Peng X., Tiziani H. '*Geometry for contouring by electronic speckle pattern interferometry based on shifting illumination beams*', Applied Optics **31** (31) 6616-6621 (1992).

13. Rodriguez-Vera R., Kerr D., Mendoza-Santoyo F. '*Electronic speckle contouring*', Journal of the Optical Society of America A **9**(11) 2000-2008 (1992).

14. Joenathan C., Pfister B., Tiziani H.J. '*Contouring by electronic speckle pattern interferometry employing dual beam illumination*', Applied Optics **29**(13) 1905-1911 (1990).

15. Abramson N. '*Holographic contouring by translation*', Applied Optics **15**(4) 1018-1022 (1976).

16. Carelli P., Paoletti D., Schirripa Spagnolo G., de Altorio A. '*Holographic contouring method: application to automatic measurements of surface defects in artwork*', Optical Engineering **30** 1294-1298 (1991).

17. de Mattia P., Fossati-Bellani V. '*Holographic contouring by displacing the object and the illumination beam*', Optics Communications **26** 17-21 (1978).

18. Rastogi P.K., Pflug L. '*A holographic technique featuring broad range sensitivity to contour diffuse objects*', Journal of Modern Optics **38**(9) 1673-1683 (1991).

19. Yonemura M. '*Holographic contour generation by spatial frequency modulation*', Applied Optics **21** 3652-3658 (1982).

20. Zelenka J.S., Varner J.R. '*Multiple-index holographic contouring*', Applied Optics **8** 1431-1434 (1969).

21. Friesem A.A., Levy U. '*Fringe-formation in two-wavelength contour holography*', Applied Optics **15** 3009-3020 (1976).

22. Haines K.A., Hildebrand B.P. '*Contour generation by wavefront reconstruction*', Physics Letters **19** 10-11 (1965).

23. Heflinger L.O., Wuerker R.F. '*Holographic contouring via multifrequency lasers*', Applied Physics Letters **15** 28-30 (1969).

24. Hildebrand B.P., Haines K.A. '*The generation of three-dimensional contour maps by wavefront reconstruction*', Physics Letters **21** 422-423 (1966).

25. Hildebrand B.P., Haines K.A. '*Multiple-wavelength and multiple-source holography applied to contour generation*', Journal of the Optical Society of America **57** 155-162 (1967).

26. Tatam R.P., Davies J.C., Buckberry C.H., Jones J.D.C. '*Holographic surface contouring using wavelength modulation of laser diodes*', Optics & Laser Technology **22**(5) 317-321 (1990).

27. Varner J.R. '*Simplified multiple-frequency holographic contouring*', Applied Optics **10** 212-213 (1971).

28. Zelenka J.S., Varner J.R. '*New method for generating depth contours holographically*', Applied Optics **7** 2107-2110 (1968).

29. Hecht E. 'Basics of coherence theory' in *Optics*, Addison-Wesley Publishing Company, Reading, USA, 2nd ed, 1974, pp. 516-537.

30. Dresel T., Hausler G., Venzke H. '*Three-dimensional sensing of rough surfaces by coherence radar*', Applied Optics **31**(7) 919-925 (1992).

31. Takeda M., Yamamoto H. '*Fourier-transform speckle profilometry: three-dimensional shape measurements of diffuse objects with large height steps and/or spatially isolated surfaces*', Applied Optics **33**(34) 7829-7837 (1994).

32. Kikuta H., Iwata K., Nagata R. '*Distance measurement by the wavelength shift of laser diode light*', Applied Optics **25**(17) 2976-2980 (1986).

33. Barnes T.H., Eiju T., Matsuda K. '*Rough surface profile measurement using speckle optical frequency domain reflectometry with an external cavity tunable diode laser*', Optik **103**(3) 93-100 (1996).

34. Tiziani H.J., Franze B., Haible P. '*Wavelength-shift speckle interferometry for absolute profilometry using a mode-hop free external cavity diode laser*', Journal of Modern Optics **44**(8) 1485-1496 (1997).

35. Kuwamura S., Yamaguchi I. '*Wavelength scanning profilometry for real-time surface shape measurement*', Applied Optics **36**(19) 4473-4482 (1997).

36. Yamaguchi I., Yamamoto A., Kuwata S. '*Speckle decorrelation in surface profilometry by wavelength scanning interferometry*', Applied Optics **37**(28) 6721-6728 (1998).

37. Kinoshita M., Takeda M., Yago H., Watanabe Y., Kurokawa T. '*Optical frequency-domain imaging microprofilometry with a frequency-tunable liquid-crystal Fabry-Perot etalon device*', Applied Optics **38**(34) 7063-7068 (1999).

38. Takeda M., Aoki T., Miyamato Y., Tanaka H., Ruowei G., Zhibo Z. '*Absolute three-dimensional shape measurements using coaxial and coimage plane optical systems and Fourier fringe analysis for focus detection*', Optical Engineering **39**(1) 61-68 (2000).

39. Geng Z.J. '*Rainbow three-dimensional camera: new concept of high-speed three-dimensional vision systems*', Optical Engineering **35**(2) 376-383 (1996).

40. Fang Q., Zheng S. '*Linearly coded profilometry*', Applied Optics **36**(11) 2401-2407 (1997).

41. Sansoni G., Corini S., Lazzari S., Rodella R., Docchio F. '*Three-dimensional imaging based on Gray-code light projection: characterization of the measuring algorithm and development of a measuring system for industrial applications*', Applied Optics **36**(19) 4463-4472 (1997).

42. Gartner H., Lehle P., Tiziani H.J. '*New, highly efficient, binary codes for structured light methods*', Proceedings of SPIE **2599** 4-13 (1996).

43. Sansoni G., Carocci M., Rodella R. '*Three-dimensional vision based on a combination of gray-code and phase-shift light projection: analysis and compensation of the systematic errors*', Applied Optics **38**(31) 6565-6573 (1999).

44. Meadows D.M., Johnson W.O., Allen J.B. '*Generation of surface contours by moiré patterns*', Applied Optics **9**(4) 942-947 (1970).

45. Takasaki H. '*Moiré topography*', Applied Optics **9**(6) 1467-1472 (1970).

46. Idesawa M., Yatagai T., Takashi S. '*Scanning moiré method and automatic measurement of 3-D shapes*', Applied Optics **16**(8) 2152-2162 (1977).

47. Moore D.T., Truax B.E. '*Phase-locked moiré fringe analysis for automated contouring of diffuse surfaces*', Applied Optics **18**(1) 91-96 (1979).

48. Xinjin X., Atkinson J.T., Lalor M.J., Burton D.R. '*Three-map absolute moiré contouring*', Applied Optics **35**(35) 6990-6995 (1996).

49. Xinjin X., Lalor M.J., Burton D.R., Shaw M.M. '*Four-map absolute distance contouring*', Optical Engineering **36**(9) 2517-2520 (1997).

50. Srinivasan V., Liu H.C., Halioua M. '*Automated phase-measuring profilometry of 3-D diffuse objects*', Applied Optics **23**(18) 3105-3108 (1984).

51. Srinivasan V., Liu H.C., Halioua M. '*Automated phase-measuring profilometry: a phase mapping approach*', Applied Optics **24**(2) 185-188 (1985).

52. Toyooka S., Iwaasa Y. '*Automatic profilometry of 3-D diffuse objects by spatial phase detection*', Applied Optics **25**(10) 1630-1633 (1986).

53. Saldner H.O., Huntley J.M. '*Temporal phase unwrapping: application to surface profiling of discontinuous objects*', Applied Optics **36**(13) 2770-2775 (1997).

54. Valera J.D., Jones J.D.C. '*Phase stepping in projected-fringe fibre-based moiré interferometry*', Electronics Letters **29**(20) 1789-1791 (1993).

55. Hong Z., Lalor M.J., Burton D.R. '*Spatiotemporal phase unwrapping for the measurement of discontinuous objects in dynamic fringe-projection phase-shifting profilometry*', Applied Optics **38**(16) 3534-3541 (1999).

56. Kalms M.K., Osten W., Jüptner W. '*Inverse projected-fringe technique with automatic pattern adaption using a programmable spatial light modulator*', Proceedings of SPIE **3407** 483-489 (1998).

57. Takeda M., Quan G., Kinoshita M., Takai H., Takahashi Y. '*Frequency-multiplex Fourier-transform profilometry: a single-shot three-dimensional shape measurement of objects with large height discontinuities and/or surface isolations*', Applied Optics **36**(22) 5347-5354 (1997).

